Available online at www.sciencedirect.com
SCIENCE DIRECT
Catalysis Today 105 (2005) 598–604
CATALYSIS TODAY
www.elsevier.com/locate/cattod

Transport and reaction in catalytic wall-flow filters

J.F. Knoth [a], A. Drochner [a], H. Vogel [a,*], J. Gieshoff [b], M. Kögel [b], M. Pfeifer [b], M. Votsmeier [b]

[a] *Ernst-Berl-Institut für Technische und Makromolekulare Chemie, Technische Universität Darmstadt, D-64287, Germany*
[b] *Umicore AG & Co. KG, Hanau-Wolfgang, D-63403,Germany*

Abstract

Diesel particulate filters composed of so-called wall-flow monoliths are well established devices for diesel particulate abatement. Recent improvements in production technology allow implementation of full-featured catalyst functionality in the filter walls.

From a reactor engineering point of view such wall-flow reactors with wall-integrated catalyst show fundamental differences compared to conventional flow-through monoliths. The complex interactions of convection, diffusion and reaction in the wall-flow monolith are studied by means of numerical simulation. A two-dimensional model for the flow in one pair of inlet/outlet channels with a generic first order reaction in the catalytic filter wall is developed. Concentration profiles in the reactor and a conventional flow-through catalyst are compared.

It is found that in the range of moderate reactor conversion concentration gradients along the inlet channel of the filter are small. Thus the reactor can be described by an approximate one-dimensional model, taking into account only the radial flux through the filter wall and assuming a constant inlet concentration in axial direction along the inlet channel.

Light-off curves are computed for the wall-flow and for the conventional flow-through monolith. Significantly better conversion is found for the wall-flow configuration. This can be explained by mass transfer limitation in the conventional flow-through monolith.

Keywords: Wall-flow monolith; Diesel particulate filter; Fluid dynamic; Simulation; Modeling

1. Introduction

Diesel particulate filters are well established tools for the reduction of particulate emissions from diesel exhaust [1,2,3a]. Today, diesel particle filters usually consist of ceramic monoliths with alternately blocked inlet and outlet channels. Thus the exhaust gas is forced through the wall and the soot is collected on the surface of the inlet channels. Monoliths designed like this are therefore referred to as ‘wall-flow monoliths’.

The major technological challenge for the application of particulate filters in passenger cars is the controlled regeneration of the filters by periodic oxidation of the soot at increased temperatures. The soot ignition temperature for the uncatalyzed oxidation of diesel soot is above 600 °C [3b]. This temperature can be lowered by catalytic activation of the soot. For this purpose the catalyst can either be introduced directly into the soot utilizing a fuel additive or otherwise a ceramic filter with a catalytic coating can be used. The later design is generally referred to as a ‘catalyzed particulate filter’.

Catalyzed particulate filters well known for many years are currently employed in a number of series production vehicles [4]. Early work on catalytically activated particulate filters focused entirely on the coating’s ability to support filter regeneration. Recent development aimed at the expansion of the catalytic filter functionality. Due to latest improvements in the production process, most of the conventional catalyst functionalities now can also be implemented in the wall of a particulate filter.

From the reaction engineering point of view, the wall-flow filter and the conventional flow-through catalyst are fundamentally different systems. Intuitively, the differences are obvious: In the conventional flow-through monolith convective mass transport through the reactive medium is

* Corresponding author. Tel.: +49 6151 1621 65; fax: +49 6151 1634 65.
E-mail address: vogel@ct.chemie.tu-darmstadt.de (H. Vogel).

0920-5861/$ – see front matter © 2005 Elsevier B.V. All rights reserved.
doi:10.1016/j.cattod.2005.06.050

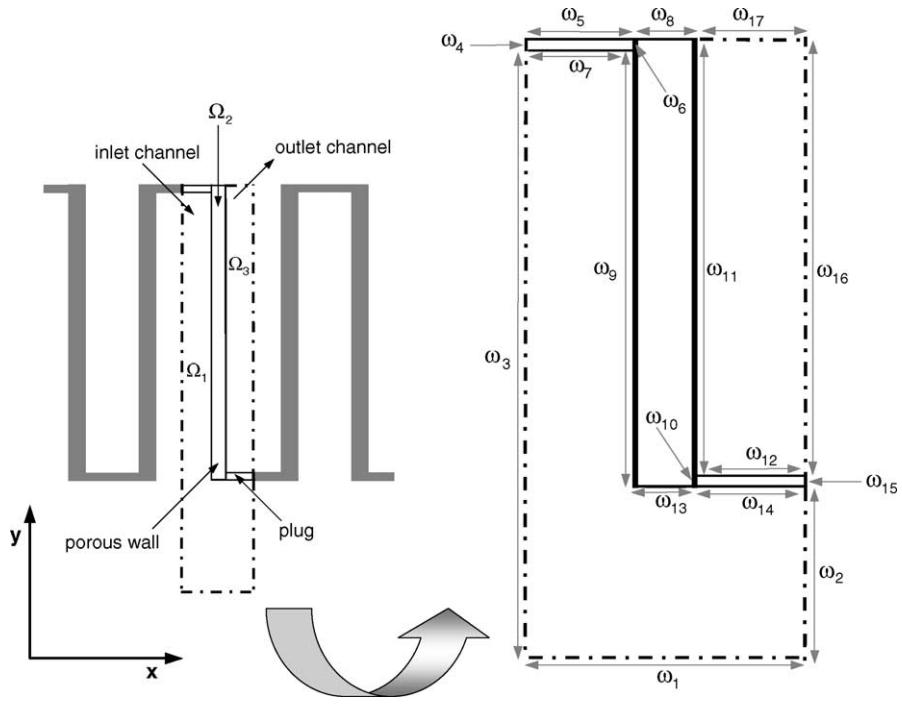

Fig. 1. Computational domains and boundaries for the 2D model (up scaled graph at the right).

impossible. Usually, the reaction is mass transfer limited by diffusive transport of the reactants into and out of the washcoat. Furthermore the reaction coordinate is oriented along the channels (*y*-direction, Fig. 1). In contrast the reactants are forced through the catalytically active wall in the wall-flow filter case. Thus, the mass transport into the reactive medium is a combination of convective and diffusive transport. Depending on the relative importance of convection and diffusion the reaction coordinate is located either along the channels (*y*-direction) or perpendicular to the channels (*x*-direction, Fig. 1).

This work focuses on numerical simulations of concentration distributions for a generic first order reaction in a clean wall-flow monolith. Thereby a fundamental understanding of the complex interaction of convection, diffusion and reaction in the wall-flow monolith reactor should be obtained. By means of the simulations the behavior of the wall-flow reactor is compared with the conventional flow-through monolith reactor.

2. Two-dimensional model

The two-dimensional model of the wall-flow monolith consists of one inlet channel (domain Ω_1), the porous wall (domain Ω_2) and one outlet channel (domain Ω_3) (Fig. 1). Due to model symmetry only one half of the inlet and outlet channels need to be considered. Dimensions of the modeled geometry are presented in Table 1.

The flow field is expressed by the Navier–Stokes Eq. (1) in the subdomains Ω_1 and Ω_3 combined with the continuity Eq. (2) [5]. The flow through the porous medium (Ω_2) is described by a combination of the continuity Eq. (2) and the Brinkman Eq. (3) [6], which is an extension of the Darcy equation. These Eqs. (1)–(3) are given below for the steady-state model:

Table 1
Dimensions of the simulated wall-flow filter, depicted in Fig. 1

Boundary	Length [mm]
ω_1	1.9
ω_2	20
ω_3	70
ω_4, ω_6, ω_{10}, ω_{15}	1
ω_5, ω_7, ω_{12}, ω_{14}, ω_{17}	0.77
ω_8, ω_{13}	0.36
ω_9, ω_{11}, ω_{16}	50

$$\rho \cdot (\mathbf{u} \cdot \nabla)\mathbf{u} = -\nabla p + \eta \cdot \Delta \mathbf{u} \quad (1)$$

$$\nabla \cdot (\rho \cdot \mathbf{u}) = 0 \quad (2)$$

$$-\eta \cdot \Delta \mathbf{u} + \kappa \mathbf{u} = -\nabla p. \quad (3)$$

The Nabla-operator ($\bigtriangledown$) represents the first order spatial derivatives, and the Laplace-operator (Δ) stands for the second order spatial derivatives, p denotes the excess pressure. Density is calculated by the ideal gas law. To calculate the dynamic viscosity (η), experimental data for air are used [7] and constant value of 0.55 μm^2 is assumed for the permeability (κ).

The following boundary conditions were used to solve the impulse balances (Table 2). Where **g** is the tangential vector

Table 2
Boundary conditions for the flow field

Navier–Stokes equations	
ω_1	$\mathbf{u} = \mathbf{u}_0$
ω_9, ω_{11}, ω_{13}	$p_{\text{Navier–Stokes}} = p_{\text{Brinkman}}$; $\eta(\nabla\mathbf{u})\mathbf{n} = 0$
ω_7, ω_{12}, ω_{14}	$\mathbf{u} = 0$
ω_2, ω_3, ω_{16}	$\mathbf{n}\cdot\mathbf{u} = 0$; $\mathbf{g}\cdot\eta(\nabla\mathbf{u}) = 0$
ω_{17}	$p = 0$; $\mathbf{g}\cdot\mathbf{u} = 0$; $\mathbf{n}\cdot(\eta\nabla\mathbf{u}) = 0$
Brinkman equations	
ω_9, ω_{11}, ω_{13}	$\mathbf{u}_{\text{Brinkman}} = \mathbf{u}_{\text{Navier–Stokes}}$
ω_6, ω_8, ω_{10}	$\mathbf{u} = 0$

and **n** the normal vector to the corresponding boundary. A constant inlet *y*-velocity v_0 is used. The lateral boundaries of the computational model obey the symmetry condition and the boundaries to the plugs follow the no-slip condition. Pressure and velocity are handed over between the Brinkman and the Navier–Stokes equation at the internal boundaries between the subdomains Ω_2 and Ω_1, Ω_3.

The steady-state mass balance (4) is valid in all three subdomains. No gas phase reaction is considered. The catalytically active wall is treated as a homogenous medium with uniformly distributed catalyst (Ω_2):

$$0 = -\nabla\cdot(c\mathbf{u}) + \nabla\cdot(D\nabla c) - r. \tag{4}$$

The model reaction rate *r* is volume based (5). In order to focus on the fundamental understanding of the reactor behavior an isothermal generic reaction with simple first order kinetics is studied:

$$r = kc = k_0 \exp\left(\frac{-E_A}{RT}\right)c. \tag{5}$$

To allow presentation of the overall conversion as a function of temperature the rate constants *k* are converted into temperatures by a power law kinetic using a typical activation energy for CO-oxidation in air ($E_A = 104\,393\ \text{J mol}^{-1}$) [8]. Due to the isothermal reaction the temperature stays constant in each simulation. However, several simulations in the temperature range from 273–673 K were performed with constant inlet velocity in order to investigate the light-off behavior (chapter 4.2).

Binary gas phase diffusion coefficients (*D* for Ω_1 and Ω_3) are calculated via the semi empirical method of Fuller et al. [9] (for CO in air). The effective diffusion coefficients in the solid phase (*D* for Ω_2) were set to $1 \times 10^{-6}\ \text{m}^2\ \text{s}^{-1}$.

Utilizing the boundary conditions given below (Table 3), a solution for the mass balance was obtained, where the inlet concentration (c_0) in the 2D model is expressed by the ideal gas law:

$$c_0 = x_0\frac{p_{\text{total}}}{RT}. \tag{6}$$

$\mathbf{N}_1$ represents the total flux vector and $\mathbf{N}_2$ describes the diffusive flux vector. It is assumed that convective mass transport is dominant at the outlet and diffusive transport through the outlet is negligible. Zero flux is implied over all other boundaries (besides in- and outlet).

Removing the plugs from the simulated wall-flow geometry and shortening the resulting geometry by 1×10^{-3} m (such that the length of the channels is again 50×10^{-3} m) leads to the geometry of the flow-through monolith. All other model properties remain identical to ensure comparability with the wall-flow model.

Models were set up and solved with the commercial software FEMLAB 3.0 a (COMSOL AB).

Several numerical calculations of the flow and pressure field in wall-flow monoliths exist in literature as well as approximate analytical solutions [2,10–13]. The flow field obtained in this work was validated against the known analytical solutions and good agreement was found. The flow field in the conventional monolith corresponds to the expected parabolic velocity profile. The linear pressure loss in the channels predicted by the Hagen–Poiseuille law is reproduced as well.

Table 3
Boundary conditions for the mass balance

ω_1	$c = c_0$
ω_2, ω_3, ω_6, ω_7, ω_8, ω_{10}, ω_{12}, ω_{14}, ω_{16}	$\mathbf{n}\cdot\mathbf{N}_1 = 0$; $\mathbf{N}_1 = -D\nabla c + c\mathbf{u}$
ω_{17}	$\mathbf{n}\cdot\mathbf{N}_2 = 0$; $\mathbf{N}_2 = -D\nabla c$

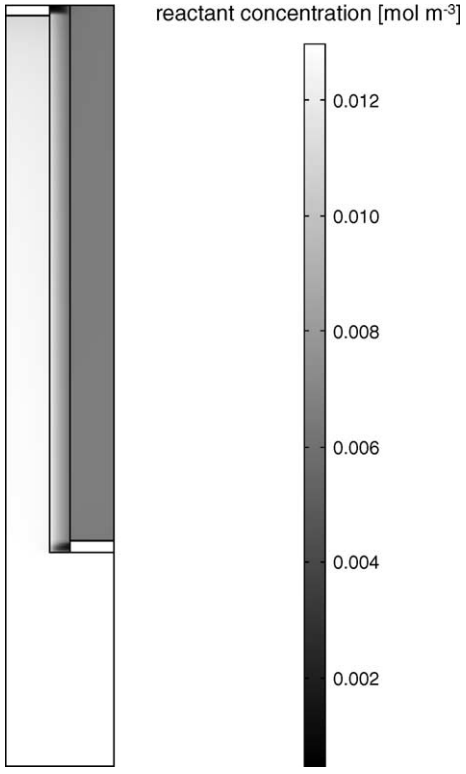

Fig. 2. Two-dimensional reactant concentration profile for the wall-flow monolith configuration ($T = 473$ K, $p = 0$, $x_0 = 500$ ppm).

3. Discussion and results

The concentration profiles in the wall-flow and the flow-through reactor model are presented and discussed in the following chapter (chapter 3.1). Light-off curves are computed based on these concentration distributions. The light-off behavior is compared and disputed in chapter 3.2. Finally, in Section 3.3 approximate one-dimensional analytical solutions for the overall reactor performance are presented.

3.1. Concentration Profiles

Solution of the coupled fluid dynamics and mass transport leads to the concentration distribution in the reactor. Fig. 2 shows the flow field in the wall-flow reactor for a rate constant of 76.59 s^{-1} and 50% overall conversion.

Nearly constant concentration profiles are observed along the *y*-coordinate in the inlet and outlet channels. The main concentration gradient is found in the porous wall in *x*-direction (parallel to the flow in the wall). The concentration

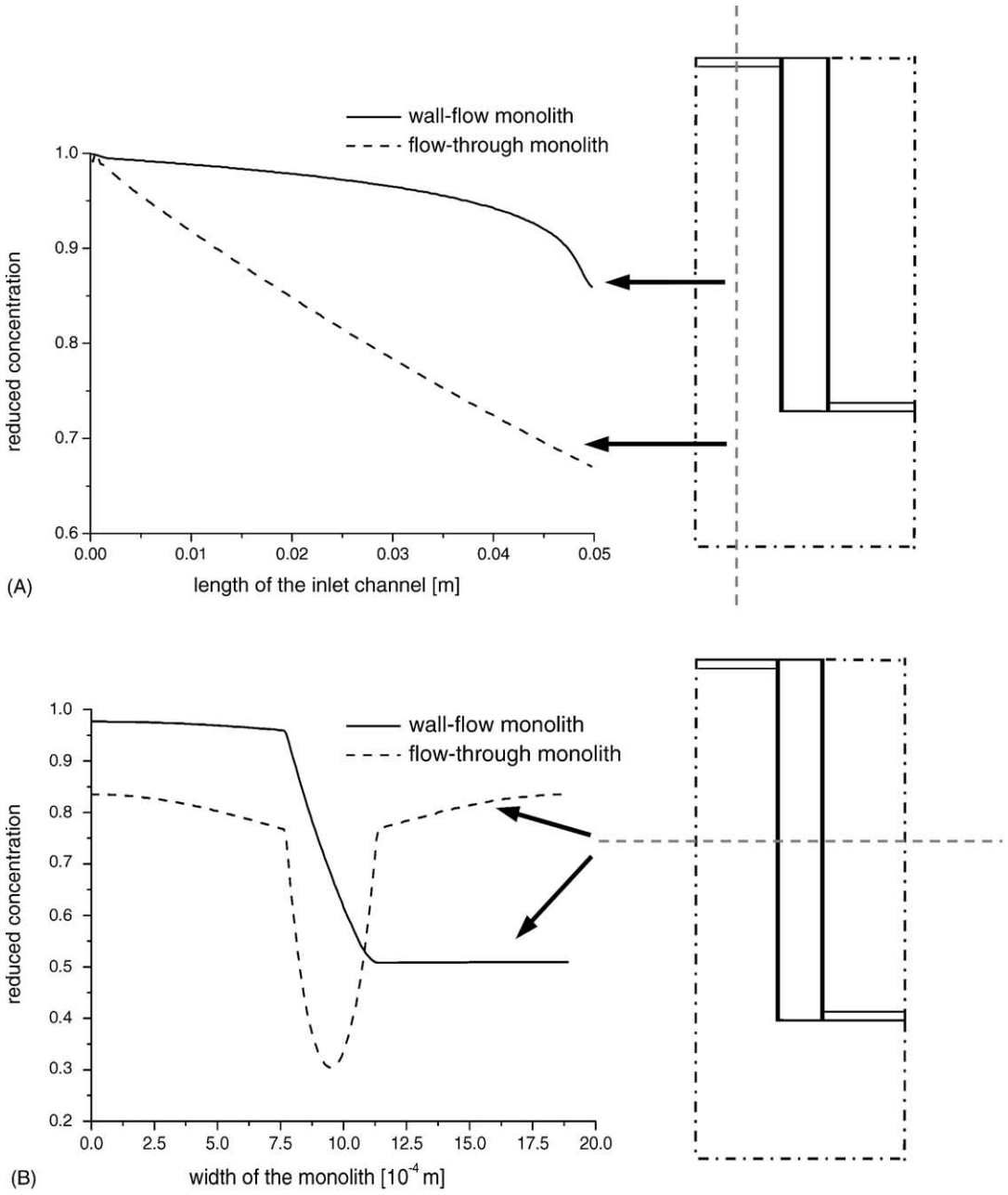

Fig. 3. (A) Reactant concentration profiles for the flow-through monolith and the wall-flow filter along the inlet channel ($T = 473$ K, $p = 0$, $x_0 = 500$ ppm). (B) Horizontal reactant distribution in the flow-through monolith and the wall-flow filter ($T = 473$ K, $p = 0$, $x_0 = 500$ ppm).

profile along the center of the inlet channel is shown in Fig. 3A, the profile in x-direction in Fig. 3B.

The small concentration gradient along the inlet channel indicates that for this condition back-diffusion (against the flow-direction in the porous wall) plays a minor role compared to the convective transport. The effect increases at the end of the inlet channel due to the decrease in axial gas velocity.

Fig. 4 shows the axial and horizontal concentration profiles for a rate constant three orders of magnitude larger than the rate constant used for the previous results. This rate constant corresponds to a temperature well above the light-off temperature of the reactor. In consequence the overall conversion at the reactor outlet approaches 100%. In this case the horizontal concentration gradient along the flow in the catalytically active wall becomes much steeper. This increases the contribution of back-diffusion against the flow-direction from the porous wall back into the inlet channel. Accordingly a strong decrease of reactant concentration along the inlet channel is observed.

3.2. Comparison wall-flow filter versus conventional flow-through monolith

Fig. 5 compares the computed overall conversion for the wall-flow reactor and the conventional flow-through

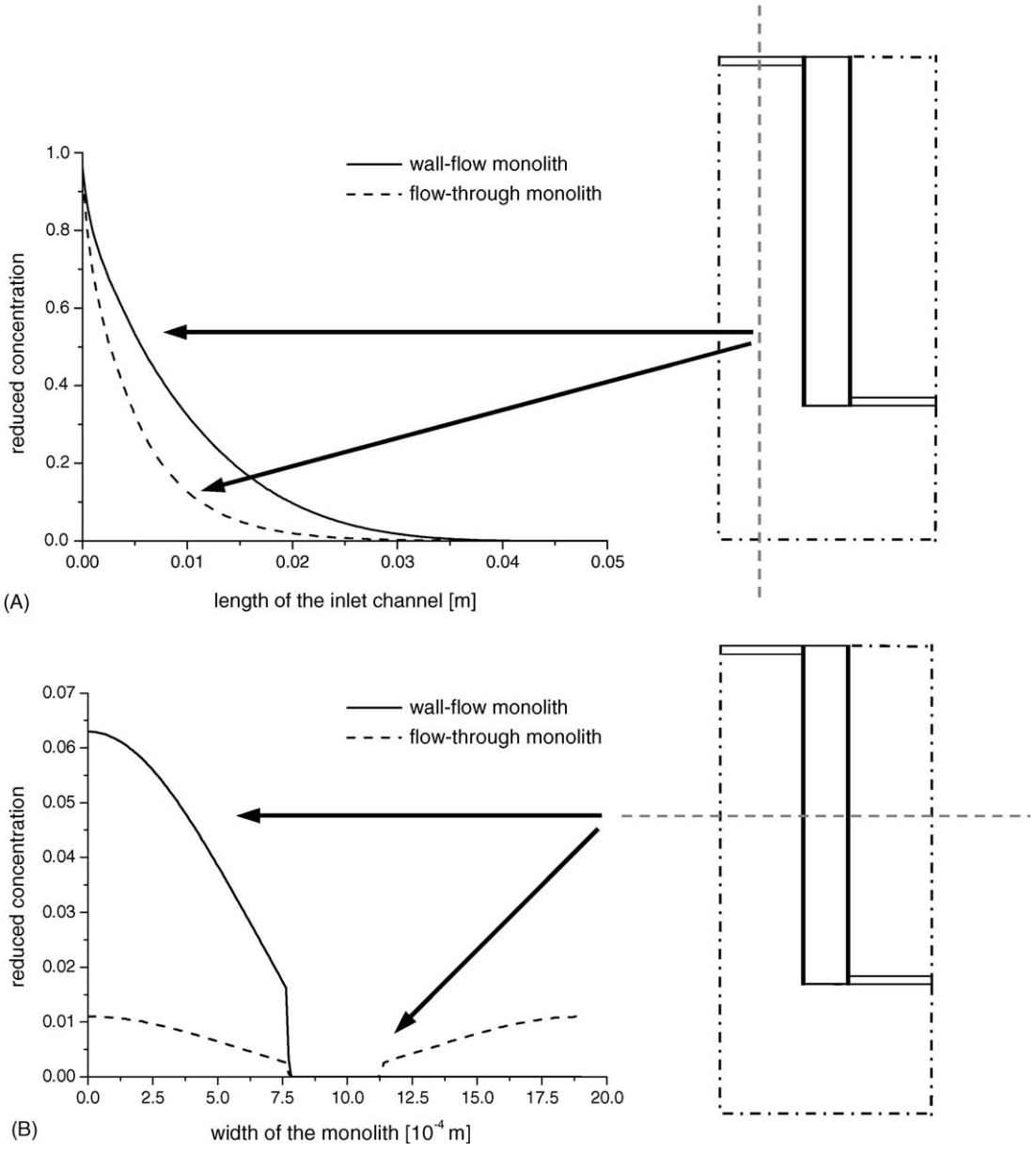

Fig. 4. (A) Reactant concentration profiles for the flow-through monolith and the wall-flow filter along the inlet channel (T = 673 K, p = 0, x_0 = 500 ppm). (B) Horizontal reactant distribution in the flow-through monolith and the wall-flow filter (T = 673 K, p = 0, x_0 = 500 ppm).

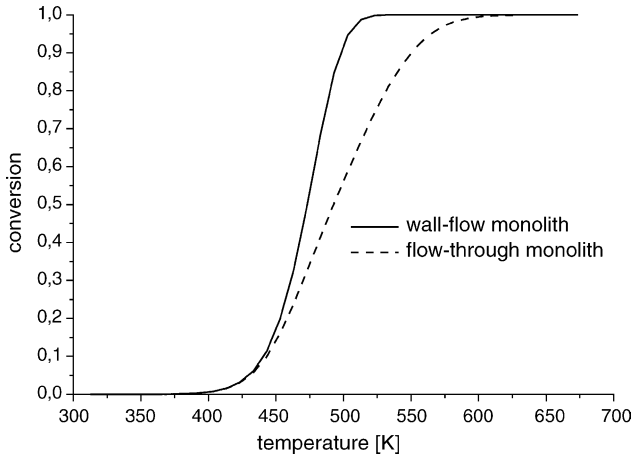

Fig. 5. Light-off behavior of the wall-flow monolith compared with the flow-through monolith ($p = 0$, $x_0 = 500$ ppm).

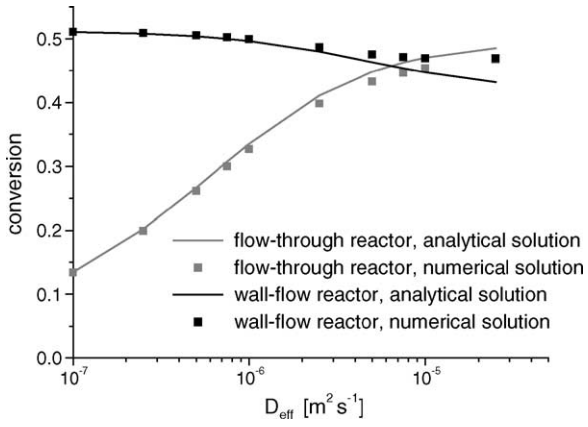

Fig. 6. Conversion in the numerical models versus the effective diffusion coefficient in the porous wall ($p = 0$, $T = 473$ K).

monolith as a function of the rate coefficient (converted to temperature using the Arrhenius Eq. (5)). The light-off temperature of the wall-flow monolith is noticeably lower than the light-off temperature of the conventional flow-through monolith. Numerical simulations agree with experimental results in the authors laboratory [14]. Both show an improved light-off behavior of the catalyzed filter compared to a conventional monolith with identical physical dimensions. An obvious explanation for the improved light-off behavior of the wall-flow reactor is mass transfer limitation of the reaction in case of the conventional flow-through monolith. The reaction in the flow-through reactor entirely depends on diffusive transport of the reactants into the catalytically active washcoat. In contrast to this, the reactants in the wall-flow configuration are forced through the wall by convection. The hypothesis that the difference in light-off behavior might be caused by mass transfer limitation in the flow-through reactor is supported by Fig. 6.

Here, conversion for both reactor configurations is compared as a function of the diffusion coefficient in the porous wall. As expected, the conversion of the conventional monolith decreases with decreasing diffusion coefficient due to diffusion transport limitation of the reaction. The conversion of the wall-flow reactor decreases slightly with increasing diffusion coefficient. This effect is discussed in the following Section 3.3.

3.3. One-dimensional analytical approximations

Simplified, approximated one-dimensional reactor models allow quick engineering calculations. Furthermore, an improved understanding via isolation of the important from the less important effects is obtained. Conventional flow-through reactors are well described by a 1D plug flow model. Effects of horizontal diffusion in the gas- and solid phase are taken into account by mass transfer coefficients and effectiveness factors based on the Thiele modulus. Diffusion in the flow direction can generally be neglected in this configuration. Fig. 6 compares the approximated conversion computed with the 1D plug flow model (neglecting axial diffusion) with the numerical solution of this work.

As shown in Section 3.1, the concentration profiles in the inlet- and outlet-channel are nearly constant in the wall-flow reactor for conditions which lead to 50% conversion. This suggests an approximate approach, where concentration gradients in the inlet and outlet channel are neglected. The concentration in the inlet channel is assumed to be equal to the reactor inlet concentration. This allows the entire reactor to be approximated by a plug flow reactor in x-direction (along the flow through the porous wall):

$$0 = -\frac{\mathrm{d}c^*}{\mathrm{d}x^*} + \frac{D}{uL}\frac{\mathrm{d}^2c^*}{\mathrm{d}x^{*2}} - \frac{kL}{u}c^* \tag{7}$$

with

$$c^* = \frac{c}{c_{\mathrm{inlet}}} \quad x^* = \frac{x}{L} \tag{8}$$

$$1 - c^* = -\frac{D}{uL}\frac{\mathrm{d}c^*}{\mathrm{d}x^*} \quad \text{at } x^* = 0 \tag{9}$$

$$\frac{\mathrm{d}c^*}{\mathrm{d}x^*} = 0 \quad \text{at } x^* = 1. \tag{10}$$

The solution of Eq. (7) with the boundary conditions (9) and (10) is described in literature [15]. In this approximation the diffusion in flow direction can not be ignored due to the small length (thickness) and slow (horizontal) flow velocity in this reactor.

Fig. 7 compares the conversion obtained with this simple analytical model with the result of the full numerical solution. The good agreement at realistic porous wall diffusion coefficients shows that the simple model captures the main effects. With higher assumed diffusion coefficients larger deviations between the simple model and the numerical solution are observed. This was expected, since the impact of back-diffusion from the porous wall into the inlet channel increases with increasing diffusion coefficient. Thus the

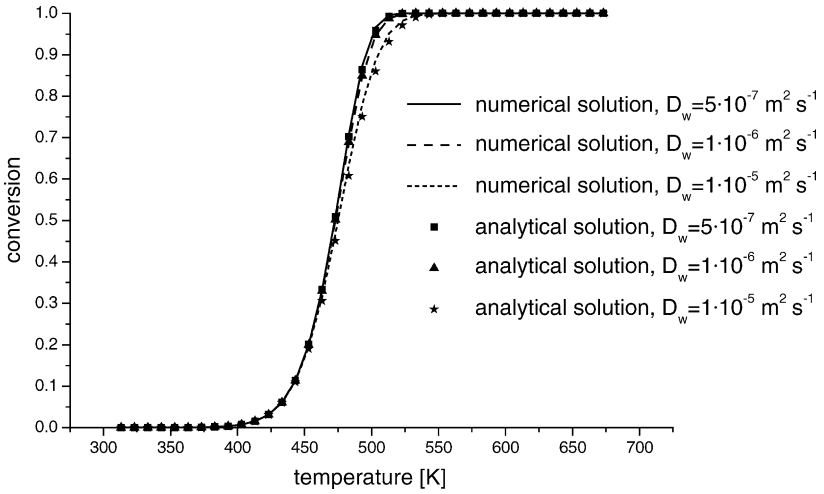

Fig. 7. Numerical and analytical calculated conversion in the wall-flow monolith ($p = 0$, $T = 473$ K).

assumption of constant inlet concentration starts to break down. It has been shown in Section 3.1 that the assumption of constant inlet channel concentration becomes invalid at higher temperatures, when the conversion approaches 100%.

4. Conclusions

A two-dimensional numerical model for the wall-flow monolith with wall integrated catalyst was established. Concentration profiles in the wall-flow monolith and the conventional flow-through monolith were calculated and compared. Despite the similar appearance, the wall-flow filter – with the given geometry and permeability – and the conventional flow-through monolith differ distinctly from the reaction engineering point of view. These discrepancies become most apparent, if the simplified 1D descriptions of the two reactors are compared. The most significant difference seems to be the orientation of the reaction coordinate. The flow-through reactor is well described by a plug-flow reactor model in y-direction. Diffusion and heat conductivity are known to be of little importance for this reactor type. The wall-flow reactor is best described by a plug flow reactor with the reaction coordinate in x-direction (Fig. 1). Diffusion in flow direction was shown to be of significance.

One major difference between both reactor concepts is the absence of transport limitation in the wall-flow reactor. Since the reactants are forced in this case through the reactive porous medium by convection. Absence of mass transport limitation in the wall-flow reactor leads to higher conversions and lower light-off temperatures compared to the conventional monolith.

Analysis of this work is limited to a simple first order isothermal reaction in a clean filter. Future work will extend this analysis to more complex reaction kinetics and to exothermic reactions.

If exothermic reactions and transient temperature profiles in the reactor are taken into account, the different orientation of the reaction coordinate in the two reactors is expected to have further interesting consequences.

References

[1] A.G. Konstandopoulos, M. Kostoglou, Soc. Automot. Eng. 2004-01-0693 (2004) 1–15.
[2] M. Kostoglou, P. Housiada, A.G. Konstandopoulos, Chem. Eng. Sci. 58 (2003) 3273–3283.
[3] (a) G.C. Koltsakis, O.A. Haralampous, C.K. Dardiotis, Z.C. Samaras, C.-D. Vogt, E. Ohara, Y. Watanabe, T. Mizutani, Soc. Automot. Eng. 2005-01-0952 (2005).
(b) O.A. Haralampous, G.C. Koltsakis, Ind. Eng. Chem. Res. 43 (2004) 875–883.
[4] J. Schommers, C. Enderle, R. Binz, F. Duvinage, N. Ruzicka, 25th Vienna Intern. Engine Symposium, M.L. Gaukler Werbeagentur Stuttgart,1500th ed., 2004.
[5] D. Etling, U. Müller, U. Riedel, J. Warnatz, in: H. Oertel, Jr (Ed.), Prandtl-Führer durch die Strömungslehre, 10th ed., Vieweg, Wiesbaden, 2001, p. 208, Chapter 5.
[6] J. Kaulitzky, dissertation, Gerhard-Mercator-Universität-GH Duisburg, 1999.
[7] R. Krauss, in: V.D.I. Wärmeatlas (Ed.), Verein Deutscher Ingenieure VDI Gesellschaft Verfahrenstechnik und Chemieingenieurwesen (GVC), eighth ed., Springer-Verlag, Berlin, 1997, p. 15, Chapter Db.
[8] S.E. Voltz, C.R. Morgan, D. Liederman, S.M. Jacob, Ind. Eng. Chem. Prod. Res. Develop. 12 (1973) 294–301.
[9] E.N. Fuller, P.D. Schettler, J.C. Giddings, Indus. Eng. Chem. 58 (1966) 19–27.
[10] M. Masoudi, Soc. Automot. Eng. 2002-01-1016 (2002) 191–204.
[11] A.G. Konstandopoulos, J.H. Johnson, Soc. Automot. Eng. 890405 (1989).
[12] C.N. Opris, J.H. Johnson, Soc. Automot. Eng. 980545 (1998) 149–175.
[13] A.G. Konstandopoulos, E. Skaperdas, M. Masoudi, Soc. Automot. Eng. 2001-01-0909 (2001).
[14] M. Pfeifer, M. Votsmeier, M. Kögel, P.C. Spurk, E.S. Lox, J.F. Knoth, Soc. Automot. Eng. 2005-01-1756 (2005).
[15] O. Levenspiel, Chemical Reaction Engineering, third ed., Wiley, New York, 1999 , pp. 312–315, Chapter 13.3.